RSC Sustainability

ROYAL SOCIETY OF CHEMISTRY

PAPER

View Article Online
View Journal | View Issue

Cite this: *RSC Sustainability*, 2024, **2**, 1088

Recovery of rare earth elements (Nd, Dy) from discarded hard disk magnets using EDTA functionalised chitosan†

Shruti Srivastava, Anurag Bajpai, Syed Mohammad Musthaq and Krishanu Biswas *

Rare earth elements (REEs) are crucial for advanced green technologies and other critical applications, including defence, medical devices, electronics, and catalysts. However, traditional methods of extracting REEs from electronic waste (e-waste) are energy-intensive, generating large amounts of hazardous waste. This study proposes an environmentally conscientious approach to recovering rare earth elements (Nd, Dy) from e-waste using chitosan, a biopolymer. Chitosan has exhibited excellent metal ion adsorption properties, which can be improved by immobilising its functional groups to target specific metal ions. EDTA has been used to functionalize chitosan, allowing it to chelate and recover REEs from discarded hard disk magnets. The proposed route was optimised for maximum yield of REE recovery by adjusting critical process parameters (pH, adsorption time, and temperature). The maximum adsorption was achieved for Nd and Dy, reaching 85.3% and 76.9%, respectively, from discarded computer hard disks. The efficiency of the proposed route was also evaluated based on the adsorption recovery of other impurities (Fe from Nd–Fe–B magnets). It was observed that in comparison to the high efficiency of recovery for Nd and Dy, the proposed route controls the amount of Fe recovered as an impurity with an average maximum yield of 58.73%. In summary, the proposed recovery route provides a promising alternative to conventional metallurgical methods for REE recovery, which can be environmentally intrusive.

Received 15th November 2023
Accepted 29th February 2024

DOI: 10.1039/d3su00427a

rsc.li/rscsus

Sustainability spotlight

This investigation presents a novel approach to address the reclamation of rare earth elements (Nd, Dy) from electronic waste using EDTA functionalized chitosan with high recovery efficiency, offering a sustainable and environmentally non-intrusive alternative to conventional metallurgical methods for the recovery of rare earth elements.

1 Introduction

Advancements in electronic and electric equipment (EEE) technology have significantly improved human life. However, they have also led to a considerable accumulation of electronic waste (e-waste), containing harmful metallic and non-metallic materials, posing severe risks to the environment and human health.[1,2] To mitigate these risks, proper processing and recycling of e-waste are necessary.[3] Despite its potential hazards, e-waste can also serve as valuable urban mines for critical materials, including rare earth elements (REEs), which are vital components of modern technology.[4,5] The consumption of REEs has continuously been increasing in various high-tech applications such as electric vehicle batteries, NiMH batteries, fluorescent lamps, magnets, and catalysts.[6] As a result, the e-waste recycling market is expected to grow at a compound annual rate of 11.9% and reach 102.62 billion USD by 2027, primarily due to recycling REEs.[1] The Nd–Fe–B permanent magnet, which contains approximately 30% REEs by weight, is a critical component of modern electrical and electronic devices, including computer hard drives, cell phone vibrator motors, MRIs, microwave amplifiers, generators, and wind turbines.[7,8] These magnets possess exceptional magnetic properties due to unique 3d–4f interactions between transition metals and REEs.[9] The global Nd–Fe–B magnet market has been growing at a rate of 20% annually over the past decade. Nevertheless, the rapid increase in their use has also led to a surge in demand, projected to exceed their supply soon.[10–12]

The extraction of rare earth elements (REE) by traditional mining is more intricate than the extraction of typical trace metals due to the presence of REE in various mineral formations. Shared properties among rare earths tend to make them

Department of Materials Science and Engineering, Indian Institute of Technology, Kanpur, Uttar Pradesh, India, 208016. E-mail: kbiswas@iitk.ac.in; Tel: +91-512-2596184

† Electronic supplementary information (ESI) available. See DOI: https://doi.org/10.1039/d3su00427a

interchangeable within crystalline formations. The extraction and isolation of rare earth elements necessitate substantial energy and generate hazardous by-products, particularly when employing acid leaching methods. Furthermore, main ores are commonly found to be intermingled with radioactive elements such as thorium. Mining is also accompanied by additional difficulties, such as adverse environmental effects, the production of radioactive waste, and low levels of metal concentration. Recycling or reprocessing existing e-waste rich in REEs is one of the most notable and environmentally benign solutions to simultaneously address the problems of limited REE supply, hazardous conventional REE mining methods, and growing e-waste. However, at present, the recycling of REEs from end products is exceedingly low (~1%) and the supply of REEs from limited geographies is likely to hinder technological development involving these materials. Recent research efforts have focused on treating scraps or spent Nd–Fe–B magnets as promising secondary resources for REEs, particularly Nd and Dy.[13–15] Zakotnik *et al.* used the hydrogen decrepitation technique to extract REEs from discarded Nd–Fe–B magnets and the by-product sludge generated during magnet and alloy shaping.[16] However, the oxidation of the Nd-rich product and the loss of Nd by evaporation were significant limitations of this method. Bian *et al.* used vacuum induction melting of scrap magnets in graphite crucibles to generate alloy containing RE carbides.[17] They also explored a dry chemical vapour transport technique that used NH_4Cl to selectively chlorinate rare earth metals from scrap. However, these energy-intensive pyrometallurgical approaches often result in impure REE products requiring additional purification.[18] Several hydrometallurgical processes have also been utilised to extract REEs with the desired purity level from used Nd–Fe–B magnets. Lee *et al.* successfully extracted constituent REEs from demagnetised Nd–Fe–B magnets using NaOH, HCl, HNO_3, and H_2SO_4 solutions.[19] Vander Hoogerstraete *et al.* reported the selective dissolution of REEs from roasted REE rich powder using HCl and HNO_3, followed by the precipitation of REEs through oxalic acid.[20] Sasai and Shimamura used mechano-chemical treatment with hydrochloric acid (HCl) and oxalic acid ($(COOH)_2$) to selectively recover REEs from scrap magnets.[21] However, several similar studies have reported the dissolution of iron along with REEs during leaching, resulting in reduced purity and the need for additional processing to separate REEs in their pure form.[22]

It is important to note that adsorption has gained recognition as one of the most effective methods of extracting metals from various sources due to its non-toxic nature, reusability, ease of use, and availability of natural adsorbents.[23] Several adsorbents, such as activated carbon, *b*-cyclodextrin, cellulose, chitosan, silica, titanium dioxide, and amino-carboxylic sorbents, have been studied for REE separation and preconcentration.[24] Among these, chitosan is a highly promising adsorbent material due to its wide availability and adjustability in its chemical structure.[25] Chitosan, a biopolymer derived from chitin, is a promising adsorbent material for metal ions due to its high surface area, porosity, and adjustable chemical structure. The chelating capacity of chitosan is derived from its molecular structure, which includes amino groups ($-NH_2$). The presence of these amine groups facilitates the absorption of metal cations through a chelation process. The amine groups readily undergo protonation in acidic conditions, leading to the electrostatic attraction between anions, including metal anions derived from anionic ligands or metal chelation by chloride.[26] Both the ion-exchange and chelation mechanisms are vying for chitosan's capacity to adsorb metal ions. By grafting metal coordinating groups onto the amine or hydroxyl groups in chitosan, it becomes possible to readily chemically modify these groups. This allows for the synthesis of chitosan derivatives that exhibit high selectivity in metal absorption.[27] This study proposes a green route for recovering REEs (Nd, Dy) from discarded hard disk magnets using ethylenediaminetetraacetic acid (EDTA)-functionalised chitosan. EDTA, a widely used chelating agent, enhances the adsorption capacity of chitosan due to the primary amino groups present in chitosan.[28,29] We evaluated and optimised the efficiency of the proposed method under varying conditions, such as adsorption time, pH of the stock solution, metal concentration in the stock solution, and adsorption temperature. Based on the previous discussions about the energy requirements of the pyrometallurgical process for extracting REEs and the drawbacks of alternative methods, it can be concluded that this study offers a hopeful solution for the environmentally conscientious recovery of REEs from discarded Nd–Fe–B magnets, with reusability and scalability potentials. The results indicate that this approach can either replace or complement conventional recovery methods and improve the recovery of REEs. This contributes to the advancement of a circular economy for crucial materials.

2 Experimental methods

Fig. SF1 (ESI†) schematically provides the workflow of the proposed REE recovery route. The various steps and characterisation tools utilised have been described in detail below.

2.1 Preparation of REE rich powder from discarded hard disk magnets

The Nd–Fe–B magnets utilised in the experiment were sourced from discarded Seagate Momentus ATA hard disks (ST500VTP). All hard disks of the same model were used to ensure uniformity in the results. The magnets were extracted manually from the dismantled hard disks, and the zinc coating was removed using a ceramic grinder. The magnets were then manually crushed using a mortar and pestle into smaller 3–5 mm pieces. This study employed the powder metallurgy method to recover rare earth from magnets, as depicted in Fig. SF1 (ESI).† To obtain a fine powder with a high concentration of REEs, two challenges must be overcome. The first involves demagnetising the magnets to facilitate milling and obtain a fine powder. The second entails removing the iron (Fe) that is typically present in abundance in the Nd–Fe–B magnets. The conversion of iron in the magnets to magnetite, the ferromagnetic phase, was achieved through controlled oxidation. To accomplish these goals, the magnets were initially enclosed in a quartz tube at an air pressure of 10^{-6} mbar. The Ellingham diagram[30] was used to

determine the optimal pressure and temperature for the oxidation of iron to magnetite. It was shown that this reaction can occur at a temperature of 850 °C and a pressure of 10^{-6} mbar p_{O_2}. Subsequently, the magnets were subjected to roasting cycles for demagnetisation of the magnets and controlled oxidation of iron to magnetite. Each roasting cycle comprised of heating to 850 °C followed by homogenisation for 2 hours and subsequent cooling to room temperature. The details of the roasting cycles are presented in Fig. SF2 (ESI).† The first roasting cycle led to the complete demagnetisation of the magnets beside the primary oxidation of the constituents. Subsequent roasting cycles were conducted to obtain the desired oxides. The demagnetised and oxidised magnets were further processed by mechanical milling in an Argon (Ar) atmosphere for 6 hours using a custom-made cryomill[31] cooled by liquid nitrogen to maintain a temperature of -160 ± 10 °C. Argon has been employed during cryo-milling due to its high thermal conductivity, even at very low temperatures.[32] This facilitates the maintenance of consistent and low temperatures throughout the milling operation. It is essential to achieve the necessary material attributes and promote the fragmentation of particles into smaller sizes.[32] The iron (in the form of magnetite) was then removed from the milled magnet powder by dispersing it in ethanol followed by ultrasonication for 20 minutes. Thereafter, a permanent magnet was used to attract all of the magnetite to settle at the bottom of the flask. The non-magnetic suspension was filtered. The process was iterated several times until no magnetic settlement was obtained at the bottom of the flask. The REE rich powder was then dispersed in a 98% sulphuric acid solution (10 mL for 2 g powder) and stirred for 12 hours at room temperature to obtain the stock solution for subsequent adsorption of REEs.

2.2 Functionalisation of chitosan and adsorption of REEs

The chelating ability of chitosan was improved by functionalising it with EDTA based on the procedure described by Roosen and Binnemans.[29] This study used low-viscosity chitosan obtained from shrimp shells (supplied by Sigma-Aldrich, USA) and EDTA (supplied by Merck, Germany). Initially, chitosan (5 g) was mixed with a 10% (v/v) aqueous acetic acid solution in 100 mL volume. This mixture was then diluted by adding 400 mL of methanol. Subsequently, 24 g of EDTA, suspended in 100 mL of methanol, was mixed and stirred for 24 hours at room temperature to allow the reaction with chitosan to proceed, followed by filtration. The filtered residue was then added to ethanol and stirred for an additional 12 hours, followed by filtration. The filtered residue was then mixed with a 0.1 M NaOH solution, which was added gradually to reach a pH of 11 while avoiding direct contact between functionalised chitosan and NaOH to prevent amide hydrolysis. The solution was stirred continuously for another 12 hours. The non-reacted EDTA was converted into its salt and dissolved in the aqueous phase. The functionalised chitosan was filtered, and the obtained precipitate was washed several times with demineralised water while centrifuging until the pH of the supernatant became neutral. The residue was mixed with 0.1 M HCl and washed with demineralised water until the pH of the washing water was neutral. Stirring was then conducted in ethanol, followed by filtration. Finally, the product was dried at 40 °C for 48 hours in a vacuum oven to obtain the final product, *i.e.*, EDTA-functionalised chitosan. Thereafter, the REE rich powder stock solution was mixed with EDTA-functionalised chitosan. The efficiency of the proposed method was optimised by adjusting several parameters, including the pH of the solution (using sodium hydroxide (NaOH) for increasing the pH and nitric acid (HNO_3) for lowering the pH), adsorption time, and temperature provided for adsorption. Several batch experiments were performed to determine the parameters for the maximum yield of REEs by tuning various considered process parameters.

2.3 Characterisation

X-Ray Diffraction (XRD) was utilised to investigate the phase transformations in the initial and roasted magnets using a PANalytical Empyrean diffractometer equipped with Cu-K_α radiation ($\lambda = 0.154$ nm). The XRD instrument had a power supply of 45 kV voltage and 40 mA current, and the samples were scanned in the 2θ range of 20°–80° with a scan rate of 0.5° min^{-1} and a step size of 0.01°. Scanning electron microscopy (Carl Zeiss EVO 50) with Energy Dispersive Spectroscopy (EDS) was used to obtain the chemistry and compositions of different elements in initial magnets, REE rich powder, and adsorbed elements on EDTA-functionalised chitosan. Electron Probe Microanalyzer (EPMA) with wavelength dispersive spectroscopy (WDS) was employed to quantitatively aanalyze the elements present in initial magnets and REE rich powder. The particle size distribution of the cryomilled magnet powder was measured using a Zetasizer Nano ZS 90 setup, utilising dynamic laser scattering (DLS). To achieve sufficient dispersion for DLS experiments, 0.1 g of milled magnet powder was dispersed in 10 mL of demineralised water and ultrasonicated for 25 to 30 minutes. Fourier-transform Infrared Spectroscopy (FTIR-PerkinElmer UATR Two) was used to identify the functional groups in the functionalised chitosan and chitosan with adsorbed REEs. The instrument performed an eight-time scan in the 4000–400 cm^{-1} range. Inductively Coupled Plasma Mass Spectroscopy (ICP-MS) was used to determine the quantity of various metals present in the REE rich powder and the amount of metals adsorbed on the EDTA-functionalised chitosan using Thermo Fisher Scientific Icap-Q equipment. Standard solutions of Nd, Dy and Fe were used to analyze their concentration adsorbed by ffunctionalisedchitosan. To prepare a standard solution of 10 parts per million (ppm) of Dy, 0.015 g of Dy was dissolved in 12.3 microliters (μL) of nitric acid, which was then diluted in 1200 mL of demineralised water. A 10 ppm Nd standard solution was prepared by dissolving 0.0069 g of Nd in 6.41 μL of nitric acid, diluted in 690 mL of demineralised water. Calibration was performed using the standards mixed to obtain different measures ranging from 0.1, 0.5, 1, 5, 10, 25, 50, 75, 100, to 200 ppb, and 1% nitric acid was used for dilution purposes. Finally, intensity counts per second and concentration were measured, and a dilution of 2500× of the sample solution was

performed to obtain the results within calibration. The quantification was done using the inverse method. The amount of REEs left in the stock solution for different adsorption conditions was evaluated to estimate the adsorption yield for different experiments.

3 Results and discussion

3.1 From scrap Nd–Fe–B magnet to REE rich powder

X-ray diffraction (XRD) analysis was carried out to identify the various phases in the hard disk magnets, as depicted in Fig. 1(a). The pattern revealed the existence of two distinct sets of peaks, which indicate the presence of free iron (α-Fe, cubic crystal system with $a = b = c = 0.288$ nm)[33] and $Fe_{14}Nd_2B$ (tetragonal crystal system with $a = b = 0.878$, $c = 1.212$ nm)[34] phases. The investigation of different phases in the magnet is critical for devising an effective strategy for the recovery of REEs. The peaks corresponding to free iron exhibit high intensity, with the (110) peak at $2\theta = 44.53°$ being the most intense. These peaks confirm the abundance of iron in the sample, and its removal is essential for optimising the REE recovery process. SEM analysis was conducted to verify the chemical composition of the REE magnets. The SEM micrograph depicted in Fig. 1(b) was examined to determine the presence of different elements in the magnet sample *via* EPMA-WDS (wavelength dispersive spectroscopy). Since the magnets contain boron which cannot be correctly quantified by EDS owing to its low atomic number, WDS can provide an accurate quantification of elemental composition in the magnets. Twenty different samples areas were used to evaluate the elemental composition of various elements and the values were averaged out. The WDS compositional maps presented in Fig. 1(c) confirm the existence of Fe, Nd, and Dy in the magnets. Notably, the magnet is predominantly Fe-rich, followed by Nd, with only a minor quantity of Dy detected. Boron was also detected and quantified. The comparative composition of REE magnets as analysed by SEM-EDS and EPMA-WDS in weight% is provided in Table 1. The results show over 70 wt% of iron in the sample that needs to be removed during pre-processing to facilitate REE recovery. At the same time, about 27 wt% of magnets comprise REEs, namely Nd and Dy, which find good agreement with the values previously reported in the literature.[35]

In order to further validate the results obtained from SEM-EDS and EPMA-WDS, the phase fraction was quantified using the XRD results. The peaks corresponding to the different phases were fitted using the Gaussian function and the area under peaks was evaluated. The phase fraction was quantified using eqn (1).

$$\text{Phase fraction of phase A} = \frac{\sum \text{area spanned by peaks corresponding to phase A}}{\text{total area spanned by all peaks}} \quad (1)$$

Based on this, the results indicate that pure Fe corresponds to 59.83% of the sample while the remaining 41.17%

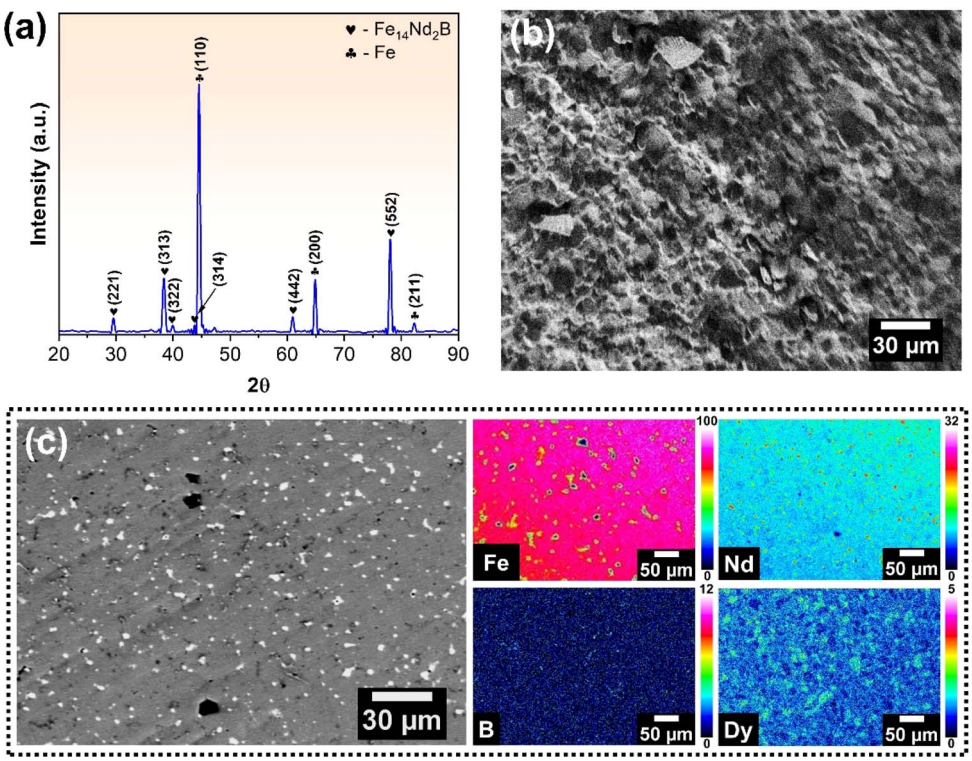

Fig. 1 (a) XRD spectra of REE magnet showing the various phases present; (b) SEM micrograph and (c) WDS maps of major constituent elements of REE magnet.

Table 1 Comparative estimation of the elemental constituents present in rare earth magnets using SEM-EDS and EPMA-WDS in weight%

Element	Weight% (SEM-EDS)	Weight% (EPMA-WDS)	Average weight%
Fe	72.78 ± 4.79	67.76 ± 2.97	70.27 ± 3.55
Nd	23.28 ± 3.86	24.41 ± 2.01	23.84 ± 0.79
Dy	3.94 ± 0.69	2.78 ± 0.87	3.36 ± 0.82
B	—	5.05 ± 0.62	5.05 ± 0.62

corresponds to $Fe_{14}Nd_2B$. This indicates that the magnets contain >70% iron, after accounting for the Fe from the $Fe_{14}Nd_2B$ phase for the compositional analyses.

The XRD and SEM analyses conducted on the REE magnets revealed a substantial amount of Fe present in the sample. To improve the efficiency of REE recovery, it is necessary to separate the Fe from the REE constituents of the magnets. Additionally, the magnetic nature of the sample poses a challenge to its conversion into a fine powder for the proposed REE recovery process. Thus, demagnetisation and controlled oxidation of the magnets were conducted before mechanical milling (explained in the Experimental methods section). The XRD patterns obtained for the REE magnet after each roasting cycle are presented in Fig. 2. It was observed that complete demagnetisation occurred after the first roasting cycle, indicating phase transformations in the magnet during roasting. The XRD plots also revealed the evolution of new phases after the first roasting cycle, with a significant fraction of Fe being converted to Fe_2O_3 (monoclinic crystal system with $a = 0.3583$ nm, $b = 0.3579$ nm, and $c = 1.672$ nm) and Fe_3O_4 (spinel crystal structure with $a = 0.8363$ nm, $b = 0.8365$ nm, and $c = 0.8376$ nm) in minor amounts.[34] Although some amount of Fe was still present in the sample, the first roasting cycle led to the transformation of the $Fe_{14}Nd_2B$ phase into two separate phases, namely $NdBO_3$ (triclinic crystal system with parameters $a = 0.629$ nm, $b = 0.657$ nm, and $c = 0.658$ nm) and $NdFeO_3$ (orthorhombic crystal system with $a = 0.546$ nm, $b = 0.564$ nm, and $c = 0.778$ nm).[33]

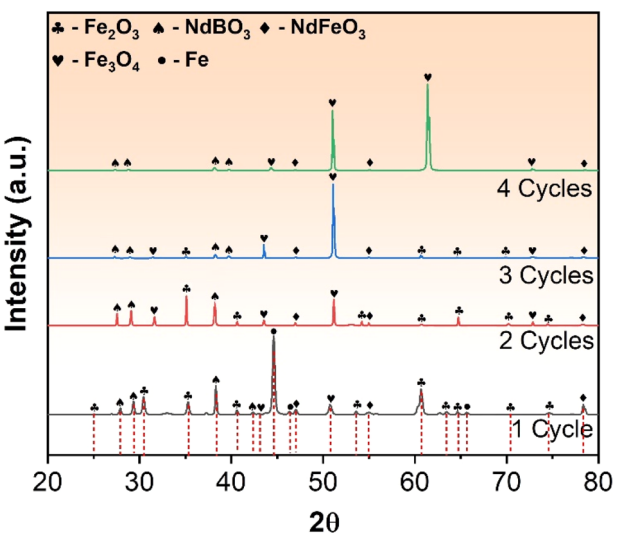

Fig. 2 XRD spectra of the evolved phases in the roasted REE magnet for each roasting cycle.

The second roasting cycle resulted in the complete conversion of Fe to Fe_2O_3 and Fe_3O_4. In the third and fourth roasting cycles, the fraction of Fe_2O_3 reduced and Fe_3O_4 increased significantly. The XRD pattern for the fourth roasting cycle confirmed the near-complete conversion of Fe to Fe_3O_4 (magnetite). Magnetite, being magnetic in nature, was separated physically using a permanent magnet, resulting in iron-deficient and REE-rich products (as explained in the Experimental methods section).

After demagnetisation and roasting, the oxidised magnets underwent cryomilling for 6 hours to convert them into a fine powder. The resulting powder was analysed for composition and morphology using SEM. Fig. SF3(a) (ESI†) presents the backscattered SEM micrograph of the cryomilled powder, revealing its typical agglomerated morphology of the resultant powder. To further analyze the size distribution of the powder particles, dynamic light scattering (DLS) was used, and Fig. SF3(b)† shows the results. The particle size ranged from 0.1 to 10 μm in size, with an average size of 2.35 ± 0.72 μm. The compositional maps of the cryomilled powder are shown in Fig. SF3(c),† and the EDS analysis confirms the retention of Nd and Dy along with Fe. The milled magnet powder was then subjected to magnetic separation to remove the iron present and obtain REE rich powder. The efficacy of the separation method used was analysed using XRD and SEM. The XRD spectrum of REE-rich powder is shown in Fig. 3(a). The pattern shows that roasting followed by cryomilling and magnetic separation results in iron-deficient powder, as indicated by the absence of any peak corresponding to Fe or its oxides. Besides, the $NdBO_3$ and $NdFeO_3$ phases are retained post magnetic separation, constituting the REE rich powder. A larger number of peaks for the $NdBO_3$ phase compared to the $NdFeO_3$ phase confirms that the powder is predominantly REE rich. The morphology and chemical composition of the REE rich powder were evaluated using SEM-EDS. Fig. 3(b) shows the backscattered SEM micrograph of REE rich powder, suggesting agglomerate morphology for the majority of the powder particles. Fig. 3(c) shows the compositional maps for various elemental constituents of the REE rich powder. The EDS analysis confirms the removal of a substantial amount of Fe from the original milled magnet powder through the proposed physical method, as evident from the compositional analysis, also summarised in Fig. 3(c). The amount of Fe significantly reduced from 70.27 ± 3.55 to 11.05 ± 0.73 wt%. To further validate the EDS results and evaluate the average bulk composition, Inductively Coupled Plasma Mass Spectrometry (ICP-MS) analysis was performed on the REE rich powder obtained after cryomilling and magnetic separation. The analysis was performed on 5 different samples, each with 5000 ppb

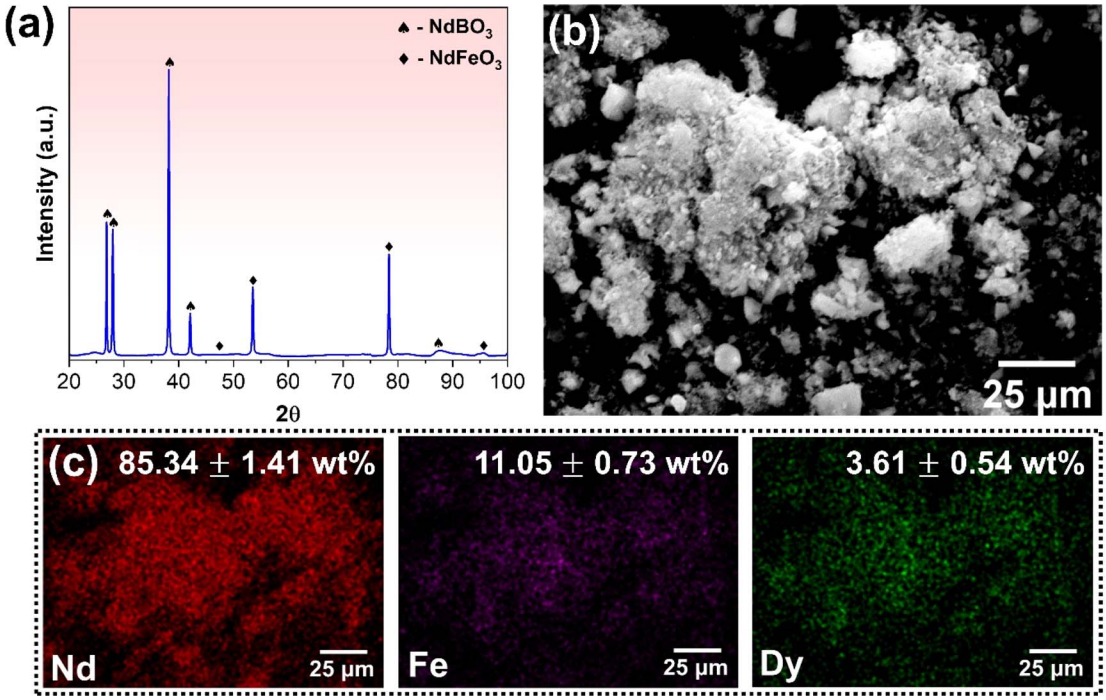

Fig. 3 (a) XRD spectrum of REE rich powder post cryomilling and magnetic separation; (b) backscattered SEM micrograph of REE rich powder along with (c) compositional maps and summary of various metals present.

concentration of the stock solution in 1% nitric acid, and the results were averaged to obtain the relative fraction of all the elements. The results indicate that the stock solution contains 4406.03 ± 23.65 ppb Nd, 432.03 ± 14.54 ppb Fe and 172.74 ± 12.78 ppb Dy, resulting in the relative concentrations of 88.10 ± 4.16% Nd, 7.63 ± 2.88% Fe and 4.27 ± 1.52% Dy. These observations agree well with the compositional analysis. The compositional analysis indicates that the processed powder is rich in REEs and deficient in Fe and thus can be used to recover REEs using the proposed route.

3.2 Functionalisation of chitosan

The functionalisation reaction between EDTA and chitosan has been schematically illustrated using Fig. SF4 (ESI).† FTIR analysis was conducted to identify the functional groups present in chitosan, EDTA, and the resultant EDTA-functionalised chitosan. Fig. 4(a) and (b) provide the FTIR spectra for chitosan and EDTA, respectively. The peaks and their corresponding functional groups have been summarised in Table 2. Chitosan has active adsorption sites such as hydroxyl groups (–OH) and primary amines ($–NH_2$). Likewise, the surface of EDTA has various active groups, as observed in its FTIR spectra, allowing it to chelate and adsorb various elements. The FTIR of the EDTA-functionalised chitosan was also performed and is shown in Fig. 4(c), indicating various functional groups present in the polymer. The spectra show the presence of –OH, $–CH_2$, –CN, –C═O, and –COOH groups in the functionalised chitosan, summarised in Table 2. EDTA is a well-known chelating agent that can form stable complexes with metal ions by binding them through its multiple carboxylic and amine functional groups. When chitosan is functionalised with EDTA, it can increase the chelation property of chitosan because of the additional chelating sites introduced by EDTA. The functionalised chitosan can now exhibit both the chelating properties of chitosan and EDTA, allowing it to form more stable complexes with metal ions. Additionally, EDTA can also increase the selectivity of chitosan, allowing it to bind to metal ions more effectively. Since chitosan is prone to degradation in acidic conditions, the ability of EDTA to sequester metal ions and buffer pH levels can help to protect chitosan from degradation to some extent.[29,36] Chitosan is a linear polysaccharide composed of repeating units of glucosamine and *N*-acetylglucosamine. The amino groups in the glucosamine units can become protonated (gain a hydrogen ion) in an acidic environment. When chitosan is exposed to acidic conditions, the protonation of amino groups can lead to further reduction on the pH and increased susceptibility to hydrolysis. Hydrolysis involves the breaking of glycosidic linkages between the sugar units that make up chitosan's polymer chain.[37] This process can result in the degradation of the chitosan molecule into smaller fragments. However, owing to the buffering effect of EDTA, there is no change in the pH due to protonation since there is an interplay between the chitosan's basic amino groups and the acidic nature of the metal–EDTA complexes formed.[38] This help maintain a relatively stable pH by reacting with excess protons or hydroxide ions in the solution, preventing drastic changes in pH and thereby reducing hydrolysis of chitosan. This has been validated in this investigation by keeping chitosan in acidic solution (H_2SO_4) of variable pH (=1, 3, 5 and 7) for 24 h. Fig. SF6 (ESI†) shows the comparative FTIR spectra of chitosan for

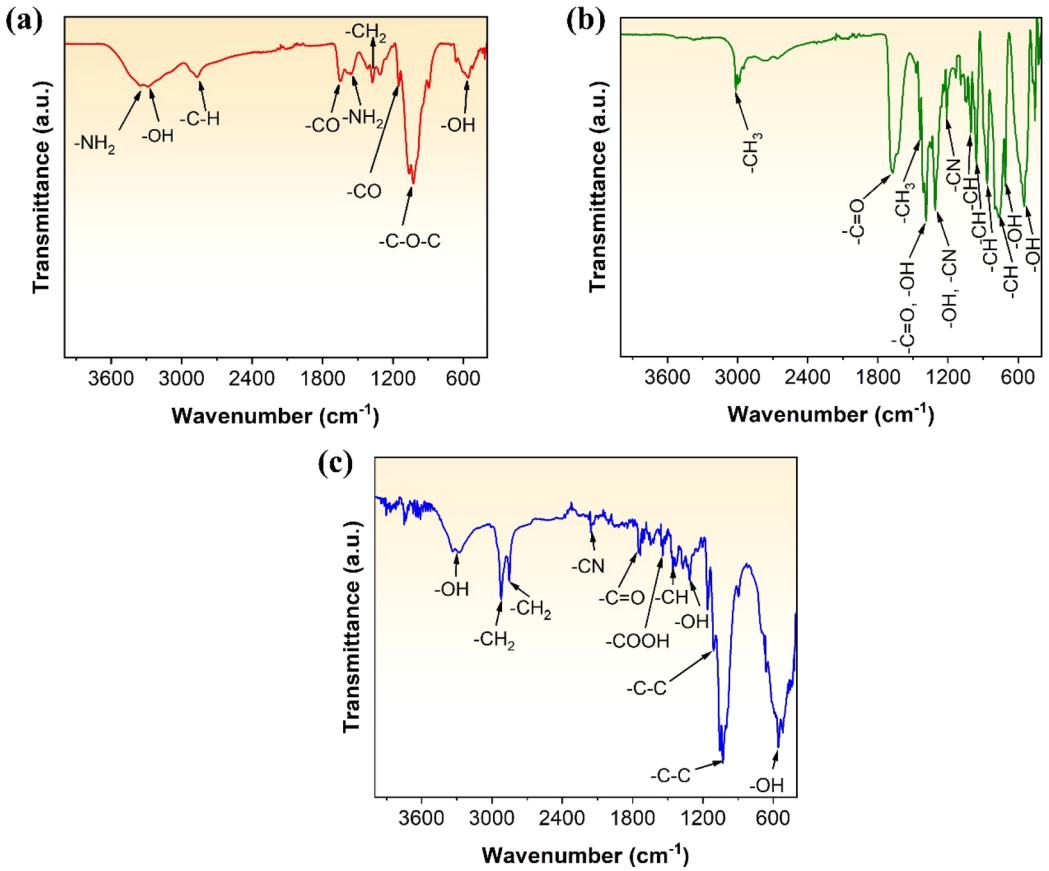

Fig. 4 FTIR spectra of (a) chitosan, (b) EDTA, (c) EDTA-functionalised chitosan.

Table 2 Functional groups and corresponding FTIR peaks for chitosan, EDTA, and EDTA-functionalised chitosan[39,40]

Functional group	FTIR peak(s) – wavenumber (cm^{-1})		
	Chitosan	EDTA	EDTA-functionalised chitosan
$–NH_2$	3346, 1592	—	—
–OH	3273, 583	1393, 1313, 711, 553	3278, 1314, 558
–CH	2859	1005, 960, 864, 785	1454
–CO	1621, 1151	1686, 1390	1747
$–CH_2$	1376	—	2922, 2852
–COC	1031	—	—
$–CH_3$	—	3013, 1438	—
–COOH	—	—	1542
–CN	—	1313, 1211	2156
–NH	—	—	—
–C–C	—	—	1105, 1027

different pH values. It is evident that while decreasing pH does not affect several chemical groups, there is clear impact of pH on the $–NH_2$ group. When pH is reduced to 5, there is a significant peak broadening for both the $–NH_2$ peaks at 3346, 1592 cm^{-1}. Further reduction in pH shows the complete dilution of the peak at 1592 cm^{-1} for pH = 1, while there is a significant peak shift for the peak 3346 cm^{-1}. The shifted peak was characterized for NH_3^+. This is consequence of increased protonation of amino group ($–NH_2$) in chitosan in highly acidic medium.[26]

3.3 Adsorption of REEs and its mechanism

The REE ions in stock solution were then adsorbed onto EDTA-functionalised chitosan using the process described in Experimental methods. The adsorption was initially performed in an acidic medium with pH = 3 for 24 hours at room temperature. The adsorbed REE ions onto EDTA-functionalised chitosan were examined using SEM. Fig. 5(a) shows the SEM micrograph for the chitosan strands and the metals adsorbed on EDTA-functionalised chitosan. Fig. 5(b) displays the high-magnification SEM micrograph for the selected region from

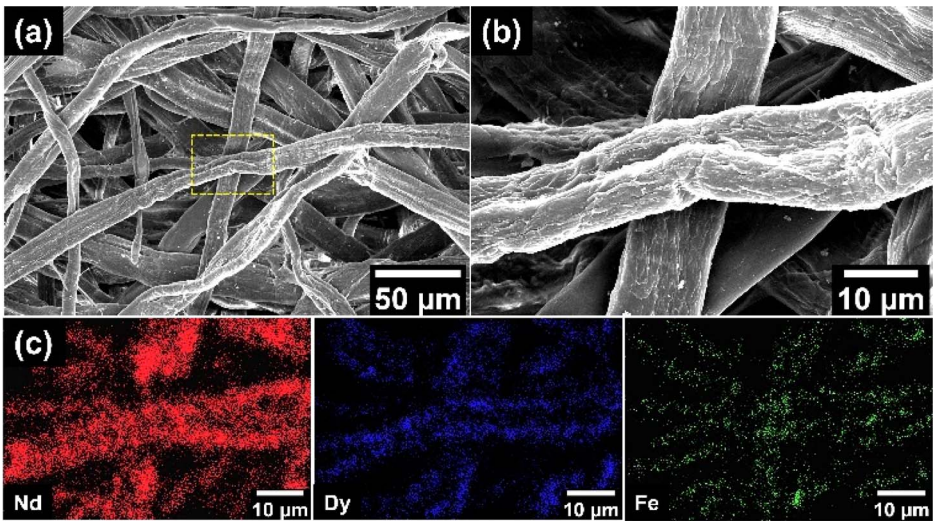

Fig. 5 (a) BSE-SEM micrograph; (b) high magnification BSE-SEM micrograph for EDTA-functionalised chitosan adsorbed with REEs; (c) EDS elemental maps for metals adsorbed onto EDTA functionalised chitosan.

Fig. 5(a). The figures show EDTA-functionalised chitosan strands intertwined with each other. Fig. 5(c) shows the compositional maps for the adsorbed metals. These maps show that Nd is the primary REE that is adsorbed onto the surface of EDTA-functionalised chitosan with significantly high coverage.

Dy also displays considerable adsorption quantities. However, the relatively small proportion of Dy in the REE rich powder is possibly the reason for its limited adsorption. There is also the existence of a trace quantity of Fe adsorbed onto the EDTA-functionalised chitosan. These results have been quantified using EDS, which indicates that 91.4 ± 2.4 at% Nd, 6.5 ± 1.1 at% Dy and 2.2 ± 0.8 at% Fe are adsorbed by EDTA-functionalised chitosan, respectively. The SEM observations serve as a visual confirmation for the adsorption of REEs by EDTA-functionalised chitosan. To validate these results, the absolute compositional fractions were further estimated for the above parameters using ICP-MS. The initial sample was approximately 2500 ppb concentration of the stock solution in 1% nitric acid which was evaluated by ICP-MS to contain 2206.03 ppb Nd, 216.02 ppb Fe and 87.78 ppb Dy. The final adsorbed results indicate that 1566.28 ppb of Nd, 97.53 ppb Fe and 58.81 ppb Dy. In relative percentages, this suggests that 90.71% is Nd, 5.64% is Fe and 3.65% is Dy of the total amount of adsorbed metals, agreeing well with the EDS results.

It is essential to comprehend the metal adsorption mechanism of chitosan, EDTA, and EDTA-functionalised chitosan to understand the results obtained using various analyses. Chitosan is a partially deacetylated acetylglucosamine polymer that is mostly composed of poly(1→4)-2 amino 2-deoxy-D-glucose units. Metal ion adsorption by chitosan is most likely achieved by chelation, which involves the production of two or more independent coordinate bonds between a polydentate ligand and a single central metal atom. The bridge model suggests that two or more amino groups from one chain bind the same metal ion. Amino sugars are the most efficient metal ion binding sites, and certain hydroxyl groups may be involved in coordination and proton release.[41] In the cation exchange mechanism, *n*-valent cationic metal ions are adsorbed on chitosan, and *n* hydrogen ions are released. Because all amino groups are protonated at pH levels less than 6, the released hydrogen ions are assumed to be protonated. Metal ions are coordinated by the nitrogen atoms of the main amino groups and the oxygen atoms of the hydroxyl groups, resulting in stable five-membered chelates of the type 1 : 2 metal : glucosamine. The great selectivity of chitosan is attributed to its flexible structure that allows for suitable configuration for complexation with metal ions.[42] A similar chelation mechanism works in the case of EDTA. The metal ion complexing molecule EDTA is also used for adsorption. It is a polyprotic acid with four carboxylic acid groups and two amine groups with lone pair electrons. The capacity of EDTA to chelate or complex metal ions in 1 : 1 metal-to-EDTA complexes is a unique characteristic. The completely deprotonated form of EDTA binds to the metal ion (all acidic hydrogens have been removed). This is EDTA working as a hexadentate ligand, meaning that all six sites of EDTA bind to the metal ion.[43] The chelation mechanisms for both EDTA and chitosan have been schematically summarised using Fig. SF5 (ESI).† Further, as discussed above, chitosan has an unusual adsorption behaviour for metal ions that can be significantly improved or augmented by chemically altering its core amino groups to provide high reactivity sites and immobilising a range of functional groups with specific affinity for certain specified metal ions.[41] When chitosan is functionalised using EDTA, three hydrogen ions are liberated for each adsorbed trivalent REE ion. This shows a cation exchange mechanism. This functionalisation of chitosan with EDTA is supposed to produce better adsorption properties than individual EDTA or chitosan.[42] EDTA also shows a buffering effect with chitosan, improving the adsorption ability. Buffering ability refers to the ability of a solution to resist changes in pH when an acid or base is added. The buffering effect are influenced by the amine groups present in chitosan that can act as weak bases. When chitosan

interacts with metal ions, it can undergo chemical reactions that lead to the liberation of hydrogen ions (protonation), causing a decrease in pH. However, when chitosan is functionalized using EDTA, there is an interplay between the chitosan's basic amino groups and the acidic nature of the metal–EDTA complexes formed. This help maintain a relatively stable pH by reacting with excess protons or hydroxide ions in the solution, preventing drastic changes in pH.[38]

3.4 Assessing sustainability of the proposed route and its optimisation

It is of utmost importance to evaluate the sustainability and efficiency of the proposed route to establish it as an environmentally conscientious solution for recovering REEs from e-waste. In the qualitative context, the use of chitosan as an adsorbent for REEs is an environmentally conscientious approach, as it is a biodegradable and renewable material. The functionalisation of chitosan with EDTA to target specific metal ions is also a green chemistry aspect of this work, as it reduces the use of hazardous chemicals and minimizes waste generation. The functionalisation of chitosan with EDTA to target specific metal ions is also a green chemistry aspect of this work, as it reduces the use of hazardous chemicals and minimizes waste generation. By functionalising chitosan with EDTA, the resulting material gains enhanced metal-binding capabilities, making it effective for selectively capturing rare earth metals from complex matrices like Nd–Fe–B magnets.[29] Further, the selectivity of chitosan–EDTA for rare earth metals minimises waste generation by avoiding unnecessary reactions with other components present in the matrix (as observed by limited adsorption of Fe owing to near complete pre-removal of Fe using roasting and magnetic separation). This targeted approach reduces the overall environmental impact associated with waste disposal. Finally, due to reduction in the degradation of chitosan by its functionalisation with EDTA, it can have optimum REE recovery yield, thereby contributing to effective reduction in use of chemicals to produce more EDTA functionalised chitosan per unit of REE recovered.[37] However, to further establish the proposed route as a viable and sustainable solution for REE recovery, it was optimised for maximum yield of recovered REEs through several experiments of varying adsorption time, temperature and pH of the solution. The amount of adsorbed REEs was analysed and quantified for each experiment using ICP-MS. Table ST1 (ESI†) summarises the adsorption yield for Nd and Dy using the proposed route for different sets of process parameters. Fig. 6 shows a comparative analysis of the adsorption of Nd and Dy for varying pH and adsorption time at both room temperature and elevated temperature (50 °C). The results indicate that an increase in pH from 1 to 5 enhances the adsorption percentage, whereas a decrease in adsorption occurs when the pH increases to 7. The amount of Nd adsorbed onto EDTA-functionalised chitosan increases with adsorption time from 12 to 24 hours and decreases beyond 24 to 48 hours due to the degradation of EDTA-functionalised chitosan resulting from prolonged exposure to the acidic medium. The maximum adsorption yield for Nd is observed at pH = 5 with 24 hours of adsorption time, both at room and elevated temperatures. For elevated temperature conditions, the maximum yield obtained for Nd adsorption was 85.3% at pH = 5 for 24 hours of adsorption time. On the other hand, the room temperature maximum adsorption is also found at pH = 5 with 24 hours of adsorption, which gives an 81.25% adsorption yield for Nd. A similar analysis was performed for Dy (Fig. 6), where the maximum adsorption yield was obtained at pH = 5 with 24 hours of adsorption time, both at room temperature and elevated temperature. The maximum adsorption for Dy at room temperature has been recorded as 72.29% at pH = 5. On the other hand, the maximum adsorption yield of 76.9% has been observed for Dy at pH = 5 and adsorption time = 24 hours in elevated temperature conditions. This have been further investigated by considering different adsorption times between 18 and 36 hours. A comparative analysis of the adsorption of Nd and Dy for varying adsorption time (t = 12, 18, 20, 22, 24, 26, 30, 36, 48 hours) at T = 50 °C and pH = 5 has been shown in Fig. SF7 (ESI).† It is evident that an adsorption time of 24 hours continues to provide the maximum adsorption yield for both Nd and Dy. Further, the increase in the fraction of adsorbed Nd and Dy onto EDTA-functionalised chitosan with an increase in pH from 1 to 5 is probably a result of both ion exchange mechanisms and alterations in the chemical speciation of the metal ions. At lower values (pH = 1), the solution is highly acidic. In such acidic conditions, the chitosan releases protons (H^+ ions) due to its functionalisation with EDTA, which is a complexing agent. The protons on the chitosan can facilitate the exchange with metal ions like Nd and Dy. At low pH, these metal ions may preferentially bind to the chitosan due to the abundance of protons available for exchange.[44] As the pH increases towards 5, the solution becomes less acidic and more neutral. At higher pH values, the carboxyl groups on the EDTA may become deprotonated (lose protons), forming negatively charged carboxylate groups. These negatively charged groups can more effectively attract and bind positively charged metal ions like Nd and Dy through complexation.[45] The electrostatic attraction between the negatively charged functional groups and the positively charged metal ions is stronger, leading to increased adsorption. Further, the speciation of Nd and Dy in solution changes with pH. At lower pH, they might exist in forms that are more prone to chelation (binding) with the functional groups on the chitosan. As the pH increases, the metal ions form more stable complexes with the deprotonated functional groups on the chitosan, contributing to increased adsorption.[46] However, as pH is increased to 7 (neutral pH), the likelihood of protonation decreases, reducing the availability of sites for metal ion binding and therefore significantly reduced adsorption. An adsorption time of 24 hours, along with the parameters mentioned above, produces a yield of ~80%, significantly higher than the other prevalent REE recovery routes. In order to provide a more holistic view of the process, the adsorption results for Fe through ICP-MS have also been provided in the Fig. SF8 (ESI).† As evident, the adsorption capacity for Fe is relatively low with an average maximum adsorption efficiency of approximately 58.4%. Through the systematic removal of ≈90% Fe from the Nd–Fe–B magnets, the final powder used for adsorption contained merely 11 wt% Fe and was predominantly rich in REEs. Therefore, the adsorption was significantly less for Fe than for Nd and Dy. One

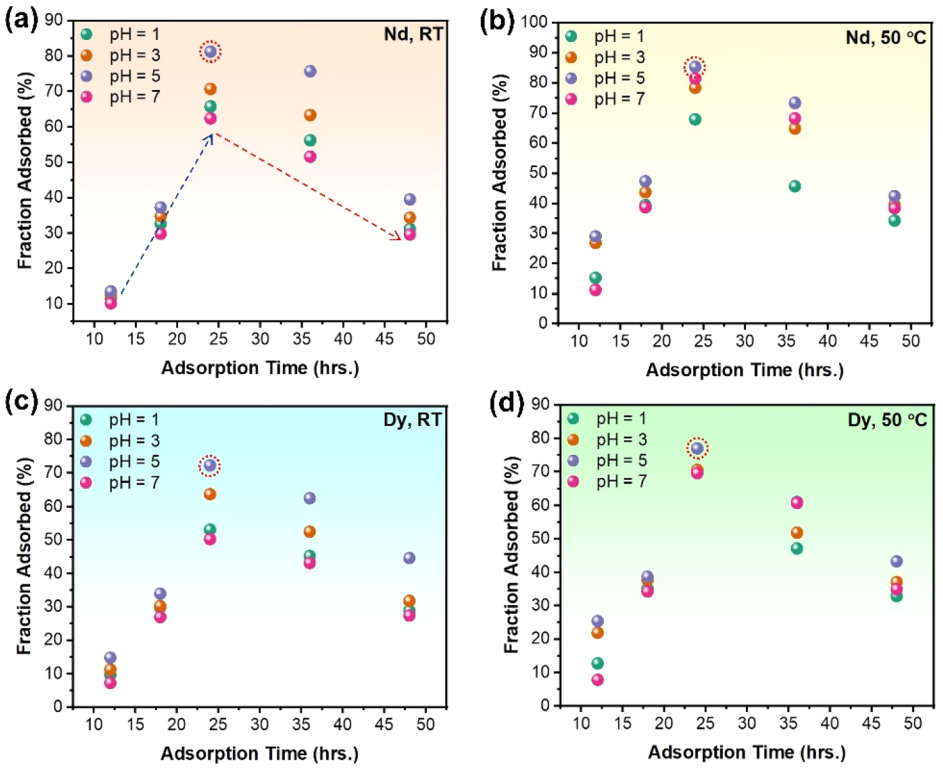

Fig. 6 Comparative analysis of fraction adsorbed of Nd and Dy at different conditions of temperature, time, and pH of the solution. (a) Nd adsorption at room temperature (RT), (b) Nd adsorption at 50 °C, (c) Dy adsorption at room temperature (RT), (d) Dy adsorption at 50 °C.

reason could be that the near complete removal of Fe to obtain REE rich powder leading to higher efficiency of REE adsorption (the limited concentration of Fe ions in the stock solution). The proposed route is, therefore, an efficient alternate strategy to recover REE from electronic waste, and the increased yield at a less acidic pH (=5) encourages the sustainable nature of the proposed REE recovery strategy.

3.5 Adsorption isotherms and thermodynamics

The adsorption isotherms could reflect the interaction pattern between adsorbent and adsorbate, further explaining the adsorption mechanisms.[47] The isotherms for the adsorption of Nd and Dy by EDTA-functionalised chitosan for various concentrations of the stock solution at 323 K with an adsorption time of 24 hours and pH = 5 (since these parameters show the maximum yield through ICP-MS analysis) are depicted in Fig. 7. It is found that the uptake capacities of both Nd and Dy increase with an increasing amount of initial concentration at the beginning and then reach a steady state beyond a certain concentration of the adsorbate. Moreover, the isotherms data of Nd and Dy on EDTA-functionalised chitosan are simulated by two well-known isotherm models, *i.e.*, Langmuir (eqn (2)) and Freundlich (eqn (3)) models,[48] and the fits are also shown in Fig. 7.

$$q_e = \frac{q_{max} K_L C_e}{1 + K_L C_e} \quad (2)$$

$$q_e = K_F C_e^{1/n} \quad (3)$$

where C_e (mg L^{-1}) represents the concentration of the adsorbate in an aqueous solution at equilibrium; q_e (mg g^{-1}) is the adsorption amount of the adsorbent at equilibrium, and q_{max} (mg g^{-1}) is the maximum uptake capacity of the adsorbent, respectively. K_L (L mg^{-1}) is a Langmuir constant concerning adsorption energy; n and K_F represent Freundlich constants associated with sorption intensity and sorption capacity, respectively. These parameters have been evaluated for both Nd and Dy and summarised in Table 3.

The higher R^2 values suggest that the Langmuir model better fits the adsorption concentration values of both adsorbates, Nd and Dy, on EDTA-functionalised chitosan. These results indicate that EDTA-functionalised chitosan has a homogeneous surface with similar sorption sites for both Nd and Dy, which were adsorbed in the monolayer form. The Langmuir monolayer uptake capacities of EDTA-functionalised chitosan for Nd and Dy at 323 K with an adsorption time of 24 hours and pH = 5 were determined to be 201.46 and 47.66 mg g^{-1}, respectively, which are considerably higher and thus relate to the higher efficiency of the proposed REE recovery route. The relatively smaller value for Dy is primarily due to its much smaller concentration than Nd in the sample.

In addition, a separation factor constant (R_L)[49] was used to evaluate the degree of suitability of EDTA-functionalised chitosan for adsorbing Nd and Dy. R_L is defined using eqn (4).

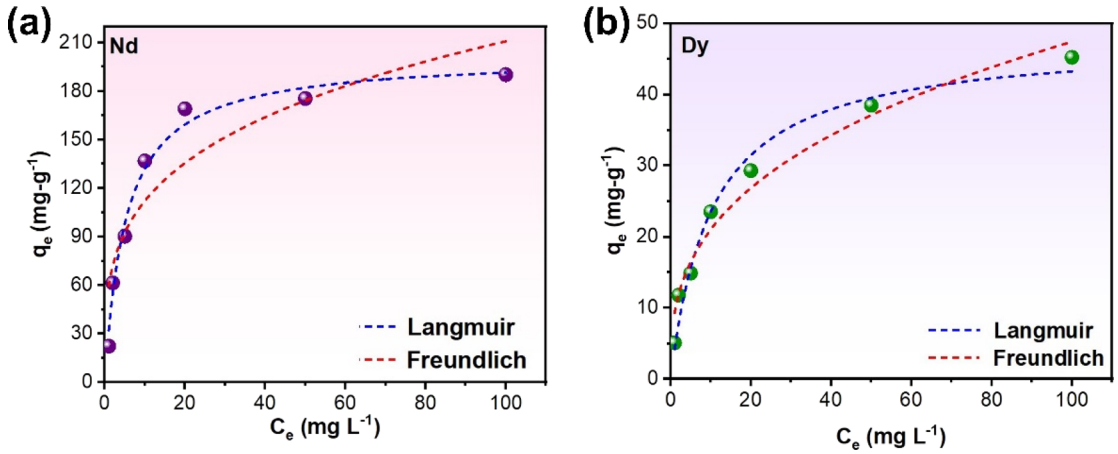

Fig. 7 Adsorption isotherm model fits for (a) Nd and (b) Dy adsorption onto EDTA-functionalised chitosan.

Table 3 Langmuir and Freundlich parameters concerning adsorption of Nd and Dy by EDTA-functionalised chitosan

	Langmuir model				Freundlich model			
Adsorbate	q_{max}	K_L	R^2	R_L	K_F	n	q_{max}	R^2
Nd	201.4	0.19	0.982	0.05–0.84	59.61	3.65	0.826	0.823
Dy	47.66	0.097	0.978	0.093–0.911	9.32	2.83	0.864	0.874

Table 4 Thermodynamic parameters for Nd and Dy adsorption by EDTA-functionalised chitosan (for $C_e = 1$)

Adsorbate	Temperature (K)	ln K_d	ΔG (kJ mol^{-1})	ΔH (kJ mol^{-1})	ΔS (J mol^{-1} K^{-1})
Nd	303	2.762	−6.91	17.94	82.02
	313	2.922	−7.73		
	323	3.204	−8.55		
Dy	303	1.289	−3.21	11.97	50.1
	313	1.503	−3.72		
	323	1.582	−4.21		

$$R_L = 1/1 + K_L C_e \quad (4)$$

where K_L (L mg^{-1}) and C_o (mg L^{-1}) represent the Langmuir constant and initial concentration of adsorbate (C_o = 0.2 mg L^{-1} here), respectively. Thus, the magnitude of R_L represents the feasibility of adsorption. The values of R_L for both Nd and Dy have also been provided in Table 3. The values of $0 < R_L < 1$ suggest the adsorption of both Nd and Dy by EDTA-functionalised chitosan is favourable.[49]

To evaluate the thermodynamic characteristics of target adsorbates (Nd and Dy) on EDTA-functionalised chitosan, the adsorption isotherms at three different temperatures (303, 313, and 323 K) were evaluated and fitted with the Langmuir model and shown in Fig. SF9 (ESI).† The data were further analysed using eqn (5) and **(6)** to obtain the thermodynamic parameters (free energy (ΔG), enthalpy (ΔH), and entropy (ΔS) of the adsorption process).[48]

$$\Delta G = -RT\ln(K_d) \quad (5)$$

$$\ln(K_d) = \frac{\Delta S}{R} - \frac{\Delta H}{RT} \quad (6)$$

where R (=8.314 J mol^{-1} K^{-1}) and T (K) are gas constant and absolute temperature, respectively. K_d is the equilibrium constant, which can be obtained using eqn (7).

$$K_d = \frac{q_e}{C_e} \quad (7)$$

where C_e (mg L^{-1}) and q_e (mg g^{-1}) are the equilibrium concentration of adsorbate (Nd or Dy) in an aqueous solution and the equilibrium uptake amount of adsorbate, respectively. ΔS and ΔH can be obtained from the intercept and slope of the plot between ln(K_d) and 1/T, respectively (shown in Fig. SF10, ESI).† The evaluated values of thermodynamic parameters are listed in Table 4. It is evident that the ΔG values at all the investigated temperatures (303, 313, and 323 K) are negative, manifesting the spontaneous adsorption process. In addition, the ΔG values decrease with increasing temperature, implying that higher temperatures are conducive to the adsorption process. Furthermore, positive values of ΔH reveal an endothermic nature of the adsorption process, and positive values of ΔS demonstrate a higher degree of randomness at the solid/liquid interface during the adsorption of Nd and Dy by EDTA-functionalised chitosan in an aqueous acidic medium.[50]

4 Conclusions

The present study presents a new methodology for extracting rare earth elements from discarded computer hard disks. This can be a stepping stone for evolving green and environmentally

conscientious techniques in the field of REE beneficiation from e-waste. Various conclusions can be made from the results and discussion presented, which are given below:

(1) Roasting combined with cryomilling emerges as a promising method for near net removal of Fe from Nd–Fe–B magnets, facilitating the adsorption of REE by EDTA-functionalised chitosan.

(2) The adsorption characterisation results indicate that EDTA-functionalised chitosan can act as a potent medium to extract REEs from e-waste with a high adsorption yield of 85.3% and 76.7% for Nd and Dy, respectively, at a reasonably elevated temperature of 50 °C and a slightly acidic environment of pH = 5 when adsorption was performed for 24 hours.

(3) The isotherm analysis reveals that the adsorption of Nd and Dy on EDTA-functionalised chitosan through the proposed route can be accurately modelled using the Langmuir model, with the monolayer adsorption capacities of 201.46 and 47.66 mg g^{-1}, respectively.

Author contributions

Shruti Srivastava: conceptualisation, investigation, methodology, analysis, and writing; Anurag Bajpai: investigation, analysis, and writing; Syed Mohammad Musthaq: investigation, and writing; Krishanu Biswas: conceptualisation, review, and supervision.

Conflicts of interest

The authors declare no conflict of interest.

Acknowledgements

The authors thank the Computer Centre, Indian Institute of Technology, Kanpur, for providing discarded hard disks to investigate this investigation. Moreover, the authors would like to thank the Department of Environmental Engineering, Indian Institute of Technology Kanpur, for providing the Inductively Coupled Plasma Mass Spectroscopy (ICP-MS) characterisation facility.

References

1 R. Nithya, C. Sivasankari and A. Thirunavukkarasu, *Environ. Chem. Lett.*, 2021, **19**, 1347–1368.
2 N. Sharma, A. Bajpai, P. K. Yadav, S. Nellaiappan, S. Sharma, C. S. Tiwary and K. Biswas, *ACS Sustain. Chem. Eng.*, 2020, **8**, 12142–12150.
3 A. Bajpai, P. Kumbhakar, C. S. Tiwary and K. Biswas, *ACS Sustain. Chem. Eng.*, 2021, **9**, 14090–14100.
4 C. Ramprasad, W. Gwenzi, N. Chaukura, N. Izyan Wan Azelee, A. Upamali Rajapaksha, M. Naushad and S. Rangabhashiyam, *Chem. Eng. J.*, 2022, **442**, 135992.
5 N. Kumar, K. Biswas and R. K. Gupta, *RSC Adv.*, 2016, **6**, 111380–111388.
6 U. K. Mudali, M. Patil, R. Saravanabhavan and V. K. Saraswat, *Trans. Indian Natl. Acad. Eng.*, 2021, **6**, 613–631.
7 A. Kumari, M. K. Jha and D. D. Pathak, *J. Environ. Manage.*, 2020, **273**, 111063.
8 J. R. Peeters, E. Bracqguene, D. Nelen, M. Ueberschaar, K. Van Acker and J. R. Duflou, *J. Cleaner Prod.*, 2018, **175**, 96–108.
9 A. Lixandru, P. Venkatesan, C. Jönsson, I. Poenaru, B. Hall, Y. Yang, A. Walton, K. Güth, R. Gauß and O. Gutfleisch, *Waste Manage.*, 2017, **68**, 482–489.
10 J. Zhang, J. Anawati, Y. Yao and G. Azimi, *ACS Sustain. Chem. Eng.*, 2018, **6**, 16713–16725.
11 Y. Mochizuki, N. Tsubouchi and K. Sugawara, *ACS Sustain. Chem. Eng.*, 2013, **1**, 655–662.
12 P. Venkatesan, T. Vander Hoogerstraete, K. Binnemans, Z. Sun, J. Sietsma and Y. Yang, *ACS Sustain. Chem. Eng.*, 2018, **6**, 9375–9382.
13 D. Kim, L. E. Powell, L. H. Delmau, E. S. Peterson, J. Herchenroeder and R. R. Bhave, *Environ. Sci. Technol.*, 2015, **49**, 9452–9459.
14 Y. Bian, S. Guo, L. Jiang, J. Liu, K. Tang and W. Ding, *ACS Sustain. Chem. Eng.*, 2016, **4**, 810–818.
15 R. Sasai, N. Shimamura and T. Fujimura, *ACS Sustain. Chem. Eng.*, 2020, **8**, 1507–1512.
16 M. Zakotnik, I. Harris and A. Williams, *J. Alloys Compd.*, 2008, **450**(1–2), 525–531.
17 Y.-Y. Bian, S.-Q. Guo, Y.-L. Xu, K. Tang, X.-G. Lu and W.-Z. Ding, *Rare Met.*, 2022, **41**, 1697–1702.
18 E. G. Polyakov and A. S. Sibilev, *Metallurgist*, 2015, **59**, 368–373.
19 J.-Y. Lee, A. K. Jha, A. Kumari, J. R. Kumar, M. K. Jha and V. Kumar, *J. Metall. Mater. Sci.*, 2011, **53**, 349–354.
20 T. Vander Hoogerstraete, B. Blanpain, T. Van Gerven and K. Binnemans, *RSC Adv.*, 2014, **4**, 64099–64111.
21 R. Sasai and N. Shimamura, *J. Asian Ceram. Soc.*, 2016, **4**, 155–158.
22 Y. Zhang, F. Gu, Z. Su, S. Liu, C. Anderson and T. Jiang, *Metals*, 2020, **10**, 841.
23 I. Anastopoulos, A. Bhatnagar and E. C. Lima, *J. Mol. Liq.*, 2016, **221**, 954–962.
24 T. Kegl, A. Košak, A. Lobnik, Z. Novak, A. K. Kralj and I. Ban, *J. Hazard. Mater.*, 2020, **386**, 121632.
25 G. Michailidou, I. Koumentakou, E. V. Liakos, M. Lazaridou, D. A. Lambropoulou, D. N. Bikiaris and G. Z. Kyzas, *Polymers*, 2021, **13**, 3137.
26 E. Guibal, *Sep. Purif. Technol.*, 2004, **38**, 43–74.
27 R. Navarro, J. Guzmán, I. Saucedo, J. Revilla and E. Guibal, *Macromol. Biosci.*, 2003, **3**, 552–561.
28 J. Ma, G. Zhou, L. Chu, Y. Liu, C. Liu, S. Luo and Y. Wei, *ACS Sustain. Chem. Eng.*, 2017, **5**, 843–851.
29 J. Roosen and K. Binnemans, *J. Mater. Chem. A*, 2014, **2**, 1530–1540.
30 J. H. E. Jeffes, in *Encyclopedia of Materials: Science and Technology*, 2001, pp. 2751–2753, DOI: **10.1016/b0-08-043152-6/00490-3**.
31 N. Kumar and K. Biswas, *Rev. Sci. Instrum.*, 2015, **86**, 083903.
32 A. Uhlir Jr, *J. Chem. Phys.*, 1952, **20**, 463–472.

33 A. Jain, S. P. Ong, G. Hautier, W. Chen, W. D. Richards, S. Dacek, S. Cholia, D. Gunter, D. Skinner, G. Ceder and K. A. Persson, *APL Mater.*, 2013, **1**, 011002.
34 D. Givord, H. S. Li and J. M. Moreau, *Solid State Commun.*, 1984, **50**, 497–499.
35 T. Minowa, *Resour. Geol.*, 2008, **58**, 414–422.
36 A. Shahzad, W. Miran, K. Rasool, M. Nawaz, J. Jang, S.-R. Lim and D. S. Lee, *RSC Adv.*, 2017, **7**, 9764–9771.
37 B. F. C. A. Gohi, H.-Y. Zeng, A. D. Pan, J. Han and J. Yuan, *Polymers*, 2017, **9**, 174.
38 A. E. Martell, in *Analytical Chemistry*, ed. T. Takeuchi, Pergamon, 1979, pp. 813–829.
39 J. Coates, *Interpretation of Infrared Spectra, a Practical Approach*, 2000, pp. 10815–10837.
40 A. Drabczyk, S. Kudłacik-Kramarczyk, M. Głąb, M. Kędzierska, A. Jaromin, D. Mierzwiński and B. Tyliszczak, *Materials*, 2020, **13**, 3073.
41 C. Gerente, V. K. C. Lee, P. L. Cloirec and G. McKay, *Crit. Rev. Environ. Sci. Technol.*, 2007, **37**, 41–127.
42 Y. Marcus, A. SenGupta and J. Marinsky, *Ion Exchange and Solvent Extraction. A Series of Advances*, Marcel Dekker, Inc., 2002, vol. 15.
43 S. A. Sinex, *EDTA-A molecule with a complex story*, University of Bristol, School of Chemistry website, 2004.
44 F. V. Pereira, L. V. A. Gurgel and L. F. Gil, *J. Hazard. Mater.*, 2010, **176**, 856–863.
45 D. A. Skoog, D. M. West, F. J. Holler and S. R. Crouch, *Fundamentals of Analytical Chemistry*, Cengage Learning, 2013.
46 F. G. L. Medeiros Borsagli, A. A. P. Mansur, P. Chagas, L. C. A. Oliveira and H. S. Mansur, *React. Funct. Polym.*, 2015, **97**, 37–47.
47 N. Kumar, K. Biswas and R. K. Gupta, *RSC Adv.*, 2016, **6**, 111380–111388.
48 B. Chen, H. Zhao, S. Chen, F. Long, B. Huang, B. Yang and X. Pan, *Chem. Eng. J.*, 2019, **356**, 69–80.
49 Y.-M. Hao, C. Man and Z.-B. Hu, *J. Hazard. Mater.*, 2010, **184**, 392–399.
50 M. Ghaedi, B. Sadeghian, A. A. Pebdani, R. Sahraei, A. Daneshfar and C. Duran, *Chem. Eng. J.*, 2012, **187**, 133–141.